Electrochemiluminescent nanostructured DNA biosensor for SARS-CoV-2 detection

Laura Gutiérrez-Gálvez [a,1], Rafael del Caño [a,c,1], Iris Menéndez-Luque [a], Daniel García-Nieto [d], Micaela Rodríguez-Peña [d], Mónica Luna [d], Teresa Pineda [c], Félix Pariente [a], Tania García-Mendiola [a,b,] and Encarnación Lorenzo [a,b,e,*]*

[a] Departamento de Química Analítica y Análisis Instrumental. Universidad Autónoma de Madrid. 28049, Madrid (Spain).

[b] Institute for Advanced Research in Chemical Sciences (IAdChem). Universidad Autónoma de Madrid. 28049, Madrid (Spain).

[c] Departamento de Química Física y Termodinámica Aplicada e Instituto Universitario de Nanoquímica. Universidad de Córdoba. 14014 Córdoba (Spain).

[d] Instituto de Micro y Nanotecnología IMN-CNM, CSIC (CEI UAM+CSIC), Isaac Newton 8. Tres Cantos. 28760, Madrid (Spain).

[e] IMDEA-Nanociencia, Ciudad Universitaria de Cantoblanco. 28049, Madrid (Spain).

*Corresponding author: tania.garcia@uam.es, encarnacion.lorenzo@uam.es

[1] Both authors contribute equally to this work.

ABSTRACT: This work focuses on the development of an electrochemiluminescent nanostructured DNA biosensor for SARS-CoV-2 detection. Gold nanomaterials (AuNMs), specifically, a mixture of gold nanotriangles (AuNTs) and gold nanoparticles (AuNPs), are used to modified disposable electrodes that serve as an improved nanostructured electrochemiluminescent platform for DNA detection. Carbon nanodots (CDs), prepared by green chemistry, are used as coreactants agents in the $[Ru(bpy)_3]^{2+}$ anodic electrochemiluminescence (ECL) and the hybridization is detected by changes in the ECL signal of $[Ru(bpy)_3]^{2+}$/CDs in combination with AuNMs nanostructures. The biosensor is shown to detect a DNA sequence corresponding to SARS-CoV-2 with a detection limit of 514 aM.

KEYWORDS: AuNMs, DNA biosensor, SARS-CoV-2.

1. Introduction

Coronavirus disease 2019, popularly known as COVID-19, is an infectious illness caused by the severe acute respiratory syndrome coronavirus 2 (SARS-CoV-2). On March 2020, when the confirmed cases of infection exceeded 118.000 in 114 countries and 4.291 deaths had been reported, COVID-19 was declared a pandemic by the World Health Organization (WHO)[1]. Since then, this pathology has caused more than 5.2 million deaths and 262 million cases worldwide, so it is an unprecedented challenge that all countries must face. Initially, a very low number of infection cases were reported due to lack of resources and incapacity to distinguish between COVID-19 and common flu [2]. However, today a great number of diagnostic methodologies for COVID-19 based on the detection of SARS-CoV-2 antigens (antigen tests) or anti-SARS-CoV-2 antibodies (serological tests), or the amplification of different parts of the virus genome are available. Within this last group, quantitative reverse transcription polymerase chain reaction (RT-qPCR) stands out, which is considered the "gold standard" for COVID-19 diagnosis [3]. Nevertheless, it is difficult to apply RT-qPCR as a mass screening technique due to its high cost, laboriousness and the need for expensive equipment and highly qualified personnel [4]. On the other hand, antigen tests are an interesting alternative for mass testing because of their low cost, portability and high specificity, but they are usually less sensitive than amplification-based methods [3]. Finally, serological tests are very sensitive, but they are also not suitable for mass diagnosis due to their cost and the need for long periods of time for data reporting and for trained personnel [5]. Taking into account all the limitations that these methodologies present, the development and implementation of different strategies that allow the early detection of COVID-19 in a selective, sensitive, reproducible, fast and cheap way is currently of great interest. In this sense, biosensors can offer a good alternative to the classic methodologies for COVID-19 detection. They present some advantages as fast response, simplicity, stability, portability, high sensibility, low cost and not highly qualified personnel. In particular, DNA biosensors offer a possibility of SARS-CoV-2 detection based on its genetic code. Despite there are some bibliography describing DNA biosensors, it is an area of great interest and its potential applications are still at its beginnings[6–9]. Among the different types of biosensor transduction, electrochemiluminescence (ECL) is a very attractive technique which has reach great interest in the last years and consists on recording the light emitted by species in the excited state, which have been generated at electrodes

through high-energy electron transfer reactions, when they return to the ground state [10]. Therefore, this technique could be considered as a combination of electrochemical and chemiluminescence strategies, so ECL harbors the wonderful advantages of both techniques [11] such as wide dynamic range [10], a spatial and temporal control of light emission, a greater selectivity due to the possibility of controlling the generation of excited states by varying the potentials applied to the electrode and non-existent background noise as no excitation light sources are used [12]. ECL may occur through the annihilation pathway or the coreactant pathway. Unlike ion annihilation ECL, in which the excited state material is reached through the reaction between the radicals generated by the same chemical species (known as luminophore), coreactant ECL needs two different precursors (luminophore and coreactant) [12]. Although several coreactants have been described, the search for new coreactants that provide improved ECL is a great deal of interest.

Recently it has been described in the literature that the analytical properties of diagnostic tests (such as specificity, selectivity, or sensitivity) can be improved by introducing nanomaterials into the device design [2]. In this context, the use of carbon nanodots (CDs), a novel cerodimensional nanomaterial, in the ECL technique has attracted much attention because they have recently been revealed to be excellent coreactants [13] due to their high charge transfer efficiency [14,15]. In addition, CDs have excellent optical properties and are biocompatible [16]. They are nanoestructures below 10 nm size and consists of a skeleton made on elements such as carbon, hydrogen, nitrogen and oxygen with a quasi-spherical shape and a set of surface functional groups (OH, COOH, NH_2, $CONH_2$) that improve its solubility in water and fluorescence [17].

On the other hand, another type of nanomaterial that have attracted the scientific interest since many years ago are gold nanomaterials. They can have a wide variety of forms and shapes (spheres, rods or triangular among others) and are consider one of the most popular nanomaterial at sensor application due to their ease of synthesis and modification, large surface area, good biocompatibility and high stability. Hence, they are a perfect choice as transducers for biosensors. In this sense, we can find several works using spherical or other shape gold nanoparticle for DNA biosensors [7,18–20] but as far as we know there have not been reported the use of mixtures of gold nanomaterials (AuNMs) of different shapes (gold nanoparticles (AuNPs) and gold nanotriangles (AuNTs)) as platforms for DNA biosensor development.

Hence, in this work we present for the first time the combination of two different nanomaterials, gold nanomaterials (AuNMs) and CDs for the development of an improved ECL DNA biosensor. The combination of both nanomaterials produces a synergic effect that enhance the ECL response, providing an efficient SARS-CoV-2 biosensing platform, based on the detection of its genetic code. SARS-CoV-2 can be detected by using target genes of the the specific viral gene regions coding for the spike protein (S), nucleocapsid protein (N), the RNA-dependent RNA polymerase (RdRp) gene, and the open reading frame 1 ab (ORF1ab) sequences. Despite all of them can be employed for the development of DNA biosensors for SARS-CoV-2 detection we have chosen ORF1ab sequences as a model target.

2. Material and methods

2.1.Chemicals

Sodium phosphate dibasic dihydrate ($Na_2HPO_4 \cdot 2H_2O$), sodium phosphate monobasic monohydrate ($NaH_2PO_4 \cdot H_2O$), sodium chloride (NaCl), sulfuric acid (H_2SO_4), sodium thiosulphate ($Na_2S_2O_3$), tetrachloroauric acid ($HAuCl_4$), double stranded calf thymus DNA activated and lyophilized (dsDNA), DNA oligonucleotides (listed in Table 1), 1,4-Dithiothreitol (DTT) and $[Ru(bpy)_3]Cl_2 \cdot 6H_2O$ were purchased from Merck (www.merckgroup.com/es-es). Tiger nut milk was used as a natural precursor for the CDs preparation. Purified water Millipore Milli-Q-System (18.2 MΩ.cm) was used for solutions preparation.

Table 1. SARS-CoV-2 ORF1ab DNA sequences used in this work.

	SARS-CoV-2 ORF1ab oligonucleotides	**Named**
Thiol- probe	5'- SH-C_6H_{10}-CCATAACCTTTCCACATACCGCAGACGG -3'	ProbeORF-SH
Thiol- probe TAMRA	5'- SH-C_6H_{10}-CCATAACCTTTCCACATACCGCAGACGG -TAMRA-3'	$ProbeORF_{TAMRA}$-SH
Complementary	5'- CCGTCTGCGGTATGTGGAAAGGTTATGG -3'	$SARS\text{-}CoV\text{-}2_C$
Non-Complementary	5'- GACCGTCGAAGTAAAGGGTTCCATA -3'	$SARS\text{-}CoV\text{-}2_{NC}$
Mutated	5'- CCGTCTGCGGTAT**C**TGGAAAGGTTATGG -3'	$SARS\text{-}CoV\text{-}2_{SM}$
Interferent	5'-C CAGGT GGAAC ATCAT CCGGT GATGC-3'	SARS-CoV-1
Interferent	5'-TTAGTCATCTGCGGGAATGCAGCATTATCT-3'	Influenza A

2.2.Instrumentation

Green synthesis of CDs was carried out in a CEM Discover LabMate™ microwave synthesis reactor. The purification of the CDs was carried out using 0.45 µm nylon syringe filters and dialysis membranes (Spectra/Por® 6, MWCO, 1 KDa) provided by General Laboratory Supplies (SGL).

Electrochemical and electrochemiluminescence experiments were performed with Metrohm screen-printed gold electrodes (AuSPE, DRP-220BT), which integrate a gold working electrode, a silver pseudoreference electrode and a gold auxiliary electrode.

Electrochemical measurements were carried out using a screen-printed electrode connector (Metrohm) as interface and Autolab (PGSTAT 30 potentiostat) from Metrohm.

Software package GPES 4.9 was used with the for the total control of the experiments and data acquisition.

SpectroECL instrument from Metrohm was used for electrochemiluminescence experiments which is composed with a bipotentiostat/galvanostat (± 4 V potential range, ± 40 mA maximum measurable current) combined with an electrochemiluminescence cell (spectral response range 340-850 nm) with a microspectrometer (CMOS). DropView SPELEC software is used in this case.

Transmission Electron Microscopy (TEM) images were aquiered using a transmission electron microscope used was a JEOL JEM 2100HT operating at 200 kV. Images were processed using the Fiji software .

Scanning Electron Microscopy (SEM) images of the electrodes and the AuNMs were taken at 2 kV and with a current of 13 pA, using a Scanning Electron Microscope VERIOS 460 from FEI.

Atomic Force Microscopy (AFM) images were acquired with a Nanotec Electrónica AFM system, in non-contact/tapping mode, using silicon cantilevers (PPP-FM Nanosensors, 2.8 N/m nominal spring constant and 75 kHz resonant frequency) in air. WSxM software [21] was used for the acquisition and processing of images.

An incident light microscope Axioskop 2 MAT (ZEISS) Fluorescence microscope with a mercury short arc lamp HBO 50 W/AC L1 (OSRAM) was used for fluorescence microscopy experiments.

All material and solutions were sterilized in a Nüve OT012 autoclave before to be used.

2.3.Procedures

2.3.1.Synthesis of carbon nanodots (CDs).

CDs were synthesized as follows: 3 mL of tiger nut milk was treated in a quartz flask under magnetic stirring for 30 min at 200 ºC using a microwave reactor maintaining a 150 W constant power and 170 psi pressure. The yellow solution obtained was kept to room temperature, filtered with 0.45 µm nylon syringe filter and dialyzed for 90 minutes to purify the CDs. Finally, they were stored at 4 ºC and protected from light.

2.3.2.Synthesis of gold nanomaterials (AuNMs).

The synthesis of gold nanomaterials (AuNMs), mixture of gold nanotriangles (AuNTs) and gold nanoparticles (AuNPs), were carried out following a seed-mediated growth procedure [22] and based on the use of $Na_2S_2O_3$ for $HAuCl_4$ reduction. Summarily, gold nanomaterials (AuNMs) were prepared by adding 25 ml of 2 mM $HAuCl_4$ to 30 mL of 0.5 mM $Na_2S_2O_3$ under vigorous stirring. Around 10 min later, 12.5 mL of $Na_2S_2O_3$ (0.5 mM) was added to the solution under vigorous stirring. Firstly, the solution turned clear and brown and finally deep red. During the first $Na_2S_2O_3$ addition, the seeds are formed and in the second addition the growth of seeds and gold nanomaterials (nanotriangles and nanoparticles) formation occurs. Finally, the solution is maintained stirring for 45 min. A mixture of spherical and triangular gold nanoparticles is obtained.

2.3.3.SARS-CoV-2 DNA oligonucleotides stock solutions preparation.

Stock solution of the thiol-modified probe were prepared following the protocol for thiol-modified oligonucleotide reduction using DTT and a NAP-10 column of Sephadex G-25, both purchased from Merck (www.merckgroup.com/es-es). Afterwards, the thiol-modified probe ($Probe_{ORF}$-SH) stock solution was prepared at a 10.0 µM final concentration in pH 7.0 with 10 mM phosphate buffer (PB). 100 µM stock solutions of the complementary sequence (SARS-CoV-2_C) and the non-complementary sequence (SARS-CoV-2_{NC}) using 10 mM PB (pH 7.0) with 0.4 M NaCl as solvent were prepared and stored at -20 ºC.

2.3.4.SARS-CoV-2 biosensor development.

2.3.4.1. Electrochemical pre-treatment of the electrode.

AuSPEs were activated by applying ten successive cyclic potential scans from -0.30 V to +1.20 V in a 0.1 M H_2SO_4 solution at 0.1 Vs^{-1}.

2.3.4.3. Surface electrode nanostructuration with synthetized gold nanomaterials.

AuSPEs were modified with the stock solution of the prepared gold nanomaterials (AuNMs), a mixture of AuNTs and AuNPs, by spraying them during 60 seconds on to the working electrode using an airbrush for and heating at 50 ºC during the modification process. Finally, Milli-Q water was used to wash nanostructured electrodes (AuSPE/AuNMs).

2.3.4.4. Immobilization of thiol-modified probe on AuSPEs nanostructured.

Nanostructured electrodes (AuSPE/AuNMs) were modified with 10.0 µL of 10.0 µM thiol-modified probe ($Probe_{ORF}$-SH) by drop casting and were kept for 24 h. To remove unabsorbed materials, they were washed with Milli-Q water. The modified electrodes were named as AuSPE/AuNMs/ $Probe_{ORF}$-SH.

2.3.4.4.5. Hybridization with the analyte sequence.

AuSPE/AuNMs/ $Probe_{ORF}$-SH electrodes were subsequently hybridized (1h at 40 ºC in humid chamber) with 10.0 µL of the analyte, a totally complementary sequence of a region of SARS-CoV-2 (SARS-CoV-2_C) genome, a single mismatched sequence or with the non-complementary sequence (SARS-CoV-2_{NC}) used as control. Finally, electrodes were washed with Milli-Q water to remove unabsorbed materials before Electrochemiluminescence detection.

Electrochemiluminescence (ECL)detection.

Electrochemiluminescence detection was carried out using CDs as coreactants and $[Ru(bpy)_3]^{2+}$ as luminophore. A solution containing 7 mM $[Ru(bpy)_3]^{2+}$ and 23 µM CDs in 0.2 M PB pH 8.0 was used to generate the ECL reaction, by applying a cyclic potential scan from 0.50 to 1.40 V at 0.01 Vs^{-1}. ECL signal and Cyclic Voltammograms were simultaneously recorded.

2.3.5. SARS-CoV-2 detection in spiked human serum samples

SARS-CoV-2 was determined in human serum samples spiked with SARS-CoV-2_C to study the matrix effect as well as to confirm the applicability of the biosensor. Human serum spiked samples were prepared at a final concentration of 50.0 pM SARS-CoV-2_C using human serum as solvent (supplied by Merk). Secondly, 10.0 µL of this solution were incubated with the thiolated probe on the electrode surface. Then, the hybridization process described above was carried out. Next, the electrodes were washed with water to remove non-adsorbed material and the ECL signal was recorded as it is described above. Finally, the SARS-CoV-2_C concentration was calculated from the ECL signal average value obtained using the external calibration plot (ECL = -12.02 log [SARS-CoV-2_C] + 453.23 (R = 0.997).

3. Results and discussion

We have previously reported the use of $[Ru(bpy)_3]^{2+}$/CDs system to detect DNA hybridization event, using electrochemiluminescent (ECL) transduction [23]. CDs can act as coreactants in the anodic ECL of $[Ru(bpy)_3]^{2+}$ since in presence of both CDs and $[Ru(bpy)_3]^{2+}$ there is an electrocatalytic process, where the intensity of the $[Ru(bpy)_3]^{2+}$ oxidation peak increases concomitantly as the cathodic peak disappears. The effect is more evident on increasing the CDs concentration (see Figure 1SI), when a fixed $[Ru(bpy)_3]^{2+}$ concentration is used. The role of CDs is similar to the TPrA in the anodic ECL of the $[Ru(bpy)_3]^{2+}$/TPrA system [24], being converted into reductive intermediates by the chemical oxidation of the oxygen-containing units by the electrogenerated $[Ru(bpy)_3]^{3+}$ [13] . The proposed mechanism is showed in Figure 2SI.

In the present work we have decided to go a step forward and combine the $[Ru(bpy)_3]^{2+}$/CDs system with gold nanomaterials (AuNMs) to improve the ECL response for the development of a selective and sensitive SARS-CoV-2 biosensor. AuNMs serve as platform for the thiolated DNA probe immobilization as well as an efficient electrochemical platform.

Therefore, the first step in this work has focused on the synthesis and characterization of the nanomaterials, CDs and AuNMs.

3.1. Synthesis and characterization of nanomaterials.

CDs were synthesized by tiger nut milk carbonization and using hydrothermal treatments in microwave reactor synthesizer, as it is explained in detail in the experimental section. Best results, considering the balance of speed and performance, were obtained with a reaction time of 30 min at a temperature of 200 ºC, maintaining a constant pressure of 170 psi and a power of 150 W. These CDs have been characterized by different techniques such as microscopic and spectroscopic techniques to elucidate their morphology, composition, and properties (see Figure 3SI). Quasi-spherical morphology with an average size of diameters of 6.5 ± 0.5 nm are observed. Besides the presence of a carbogenic core, as IR spectrum shows (see Figure 2SI), CDs also contain different surface functional groups as carbonyl, alcohols and amines groups on their surface. The X-Ray Diffraction (XRD) spectrum reveals that CDs are amorphous and the presence of lattice spacing of 0.34 nm belonging to the (002) plane of graphite (Figure 3SI).

Gold nanomaterials (AuNMs), a mixture of gold nanotriangles (AuNTs) and gold nanoparticles (AuNPs), were prepared through the seed-mediated growth method using $Na_2S_2O_3$ and $HAuCl_4$ as precursors, as is described in detail in Experimental section. As can be observed in Figure 1A, the presence of two bands at 1015 and 539 nm in the UV-visible-NIR, is associated with the formation of triangular nanoparticles (1015 nm) and spherical (539 nm) nanoparticles and confirms gold nanomaterial preparation.

The obtained AuNMs were characterized by different techniques as AFM, SEM and TEM to determine their size and morphology properties. The dimensions and morphology of the AuNMs were estimated by TEM. As can be observed in Figure 1B, triangular and spherical gold nanoparticles are observed, the triangular morphology nanoparticles have diameters from 50 to 300 nm with an average size of 150 ± 0.5 nm of lateral length (histogram of Figure 1C) whereas spherical gold nanoparticles present an average diameter of 15 ± 2 nm. AFM study of AuNMs deposited on Highly Oriented Pyrolytic Graphite (HOPG) was carried to provide information additionally to TEM images. Figures 1E and 1D confirm their triangular and spherical morphology. The profile in Figure 1F (blue line), shows an AuNT average length and height of 149 nm and 17.6 nm, respectively. In the case of AuNPs an average diameter of 12.0 nm can be observed. The morphologic AuNMs characteristics found by SEM (see Figure 1G) agree well with those observed by TEM AFM. SEM and AFM images of an HOPG (controls) with no AuNMs do not show any morphology (see Figure 4SI). Therefore, we can confirm the successful synthesis of the AuNMs, based on the results obtained above.

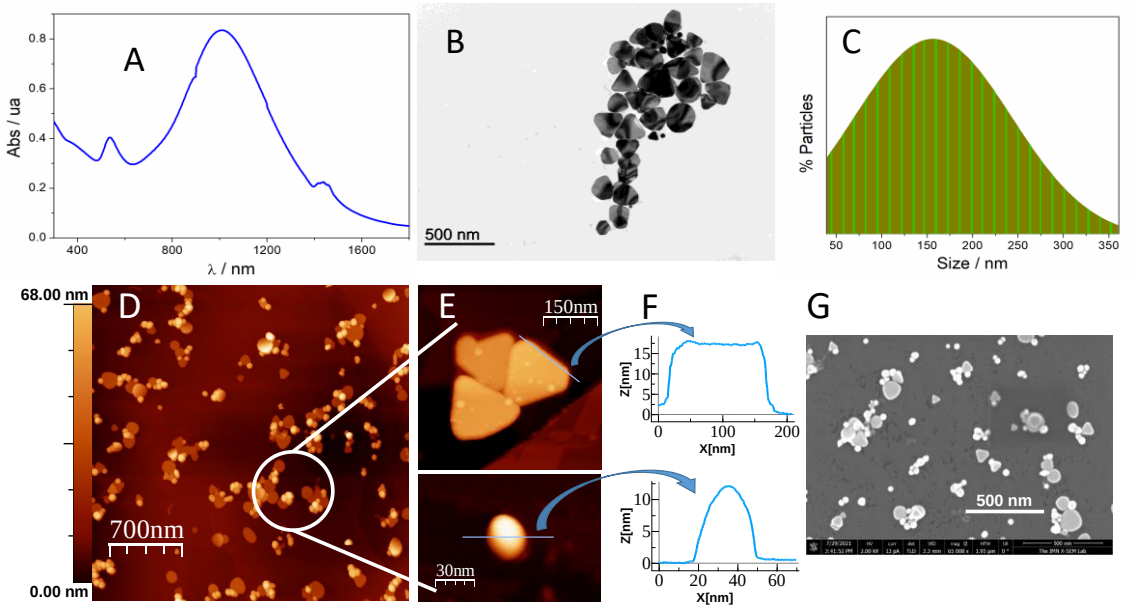

Figure 1. A) UV-visible-NIR spectra, B) TEM images, C) histogram of triangular gold nanoparticles (AuNTs), D) AFM image of AuNMs and E) magnification of AuNTs and AuNPs of the AuNMs and F), its respective profile G) SEM image of AuNMs.

3.2. Development and characterization of the biosensor.

Scheme 1 shows the development of the nanostructured electrochemiluminescent (ECL) DNA biosensor. We have prepared an efficient and simple ECL platform based on the use of AuNMs as modifiers of gold screen-printed electrodes (AuSPEs) surface and further immobilization of the capture probe on these nanostructures, as platform to develop a selective and sensitive strategy to detect characteristics SARS-CoV-2 sequences. As can be shown Scheme 1, the first step is surface modification of the AuSPE with AuNMs. Then, the hybridization of the probe-target is conducted to detect a specific DNA sequence of SARS-CoV-2, by immobilizing the thiolated capture probe (a specific thiolated sequence complementary to the target sequence) on the AuNMs. Then, the $[Ru(bpy)_3]^{2+}$/CDs ECL system was used to detect and quantify SARS-CoV-2 characteristic DNA sequences.

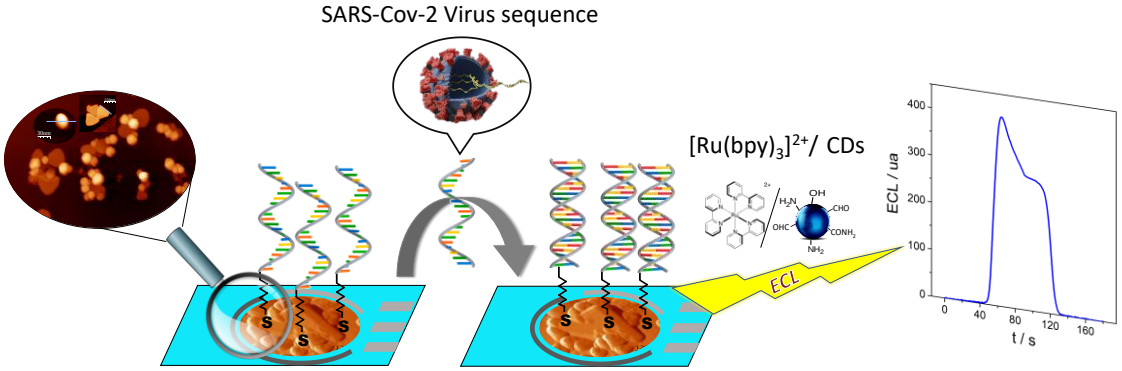

Scheme 1. Scheme of the biosensor development.

To obtain a reproducible final device, each step of the biosensor development has been characterized by SEM, AFM, Cyclic Voltammetry (CV) and ECL. Figure 2A shows the SEM image of the bare electrode, a rough surface mainly composed of Au big particles

is observed. After AuNMs modification (Figure 2B), an homogeneous distribution of the AuNMs onto the AuSPE surface is observed. AFM image (Figure 2C) of the AuSPE after AuNMs modification shows triangular and spherical particles of AuNMs corroborating SEM image and AuNMs electrode modification. Cyclic voltammograms in 0.1M H_2SO_4 after the electrode modification with AuNMs (Figure 2D) show a current increase of the gold characteristic peaks, proving AuSPE modification with AuNMs. The electroactive surface area before and after electrode modification were found to be 0.0084 and 0.0165 cm^2, respectively. This result suggests an electroactive area increment due to AuNMs immobilization on to electrode surface.

Blue line of Figure 2E and F, shows the Cyclic voltammograms and ECL signals of the $[Ru(bpy)_3]^{2+}$/CDs system at AuNMs/AuSPE and AuSPE. As can be seen, the nanostructuration of the electrode with gold nanostructures produces an increase in the electrochemical and ECL signal compared to the observed for the bare electrode (black line). This can be explained by the increase in the relative surface area and the synergistic effect that nanostructures with different shapes cause in improving electron transfer, as demonstrated by comparing with the behaviour observed when using AuNTs or AuNPS alone (see red and green lines of Figure 2 E and F). Therefore, these results demonstrate that the modification of electrodes with a combination of metallic nanostructures gives rise to improved ECL platforms. In this sense, it is reported that assembled gold or silver nanoparticles on the electrode surface can efficiently catalyze and enhance luminol ECL[25,26]. Under this premises and according with the results obtained in this work, we believe that nanostructured electrodes with combined gold nanomaterials gives rise to very stable modified electrode surfaces, with improved conductivity and a much more sensitive ECL response probably due to the catalysis the reaction of $[Ru(bpy)_3]^{2+}$ and the coreactants (CDs), enhancing ECL signal.

Optimization of CDs, pH and $[Ru(bpy)_3]^{3+}$ concentration have been carried. 23 µM of CDs, 7.0 mM $[Ru(bpy)_3]^{3+}$ and pH 8.0 were chosen as optimal conditions for further experiments.

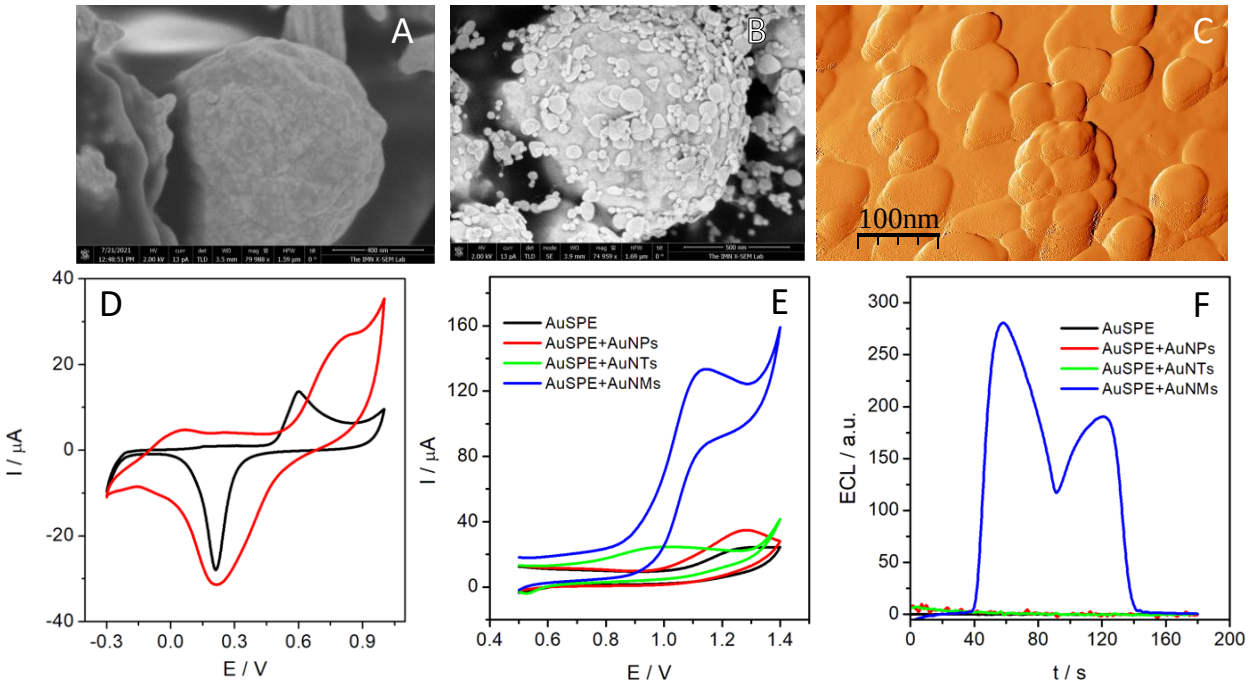

Figure 2. SEM image of AuSPE A) and AuNMs/AuSPE B). AFM image (derivative of topography) of the prepared AuNMs/AuSPE C). Cyclic voltammograms D) of a AuSPE (black line) and an AuNMs/AuSPE (red line) in 0.1M H_2SO_4. Scan rate: 100 mVs^{-1}. Cyclic voltammograms E) and ECL signal (using a 7 mM solution of $[Ru(bpy)_3]^{2+}$ + 23 µM of CDs in 0.2 M PB pH 8.0 solution) F) of a bare AuSPE (black line), an AuNMs/AuSPE (blue line), AuNPs/AuSPE (red line) and AuNT/AuSPE (green line) modified electrodes. Scan rate: 10 mVs^{-1}.

As we described above, to achieve the probe immobilization on the AuNMs surface we use a capture probe that is a complementary sequence modified on 5' extreme with a thiol (see Table 1). Thiolated capture probe immobilization on the AuNMs modified electrodes ($Probe_{ORF}$-SH/AuNMs/AuSPE) was assessed by fluorescence microscopy. In this case, in order to follow the AuNMs/AuSPE probe immobilization, a thiolated probe modified also with a fluorophore (TAMRA or tetramethylrhodamine) ($ProbeORF_{TAMRA}$-SH) was employed. As can be observed, white light optical microscope images before A) and after C) probe immobilization are quite similar. However, fluorescence images are very different since only the $ProbeORF_{TAMRA}$-SH/AuNMs/AuSPE gives a fluorescence image, confirming that the DNA probe is bound to AuNMs/AuSPE (Figure 3D). As can be observed bare AuSPE modified with AuNMs do not show any fluorescence contrast (see Figure 3C).

ECL was employed to follow the biosensor response, as well as to confirm that the thiolated capture probe was successfully immobilized on the AuNMs modified electrodes. Hence, we studied the ECL of $Ru(bpy)_3]^{2+}$/CDs at a AuNMs/AuSPE and a ProbeORF-SH/AuNMs/AuSPE, (see Figure 3E). As can be observed, after the probe immobilization there is an increase in the ECL signal compared to the small signal observed at AuNMs/AuSPE, which we believe is due to the coreactant effect of amine and hydroxyl groups present in the pirimidinic and purine bases. Therefore, these results are compatible with the capture probe immobilization on the AuNMs/AuSPE.

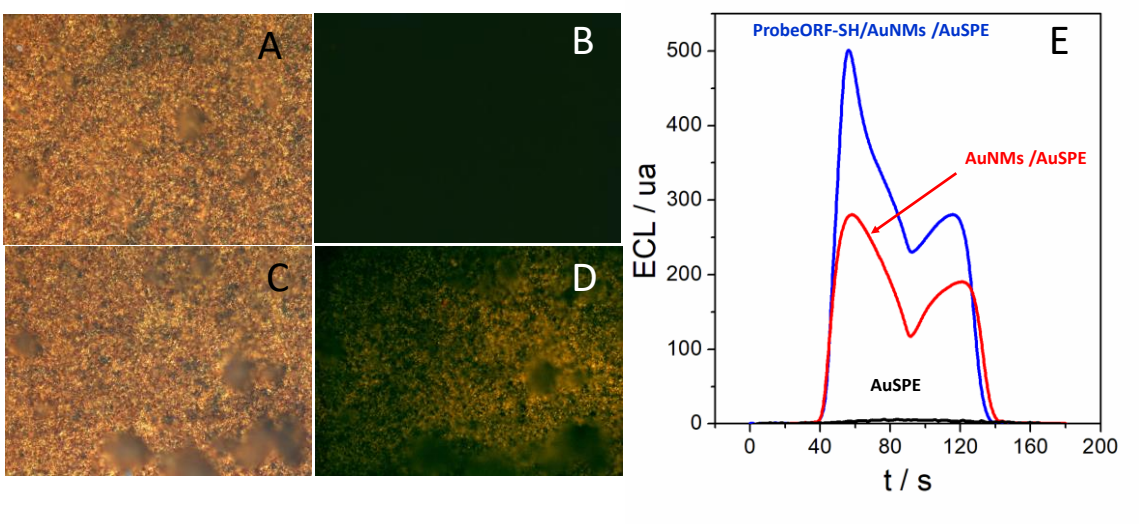

Figure 3. Optical A, C) and fluorescence B, D) images of AuNMs/AuSPE A, B) and $ProbeORF_{TAMRA}$-SH/AuNMs/AuSPE C, D). ECL signal E) of AuSPE (black line), AuNMs/AuSPE (red line) and a $ProbeORF_{TAMRA}$-SH/AuNMs/AuSPE (blue line), from 0.5 to +1.4V (vs Ag) using a 7 mM solution of [$Ru(bpy)_3]^{2+}$ and 23 µM CDs in 0.2 M PB pH 8.0. Scan rate: 10 mVs^{-1}.

3.3. SARS-CoV-2 detection.

Detection of SARS-CoV-2 was carried out by using $[Ru(bpy)_3]^{2+}$/CDs ECL system to detect hybridization event between the probe and an specific sequence from open reading frame (ORF1ab) of the virus. After DNA probe immobilization on the modified electrode surface, the hybridization with the target analyte was carried out on the biosensor surface and detected by changes in the ECL signal of $[Ru(bpy)_3]^{2+}$/CDs, enhanced by the presence of the AuNMs materials on the electrode surface.

As can be observed in Figure 4A, biosensor response before hybridization event (black bar) is higher than that observed after hybridization with the fully complementary

sequence (red bar). Particularly, hybridization of the probe produces approximately a decrease of 70 a.u in the ECL signal. However, the biosensor response to a non-complementary sequence (denoted in the text as SARS-CoV-2_{NC}) is quite similar to that obtained for the probe. As one would expect, this result confirms that hybridization process is not taking place; non specific adsorption can be the cause of the slight decrease observed.

Therefore, based on the difference of the ECL signal before and after hybridization we can affirm that the $[Ru(bpy)_3]^{2+}$/CDs ECL system can clearly detect hybridization even and the proposed methodology works well on recognizing specific DNA sequences. The different ECL signal obtained before and after the recognition reaction can be explained because hybridization event leads the formation of a stable helical conformation, which enhances the electron-transfer reaction compared to the unstructured single-stranded unit. These different DNA conformations change the $[Ru(bpy)_3]^{2+}$/CNDs ECL signal before and after hybridization as we have previously reported [23].

The analytical parameters of the DNA biosensor were calculated under the optimal experimental conditions selected before. As can be observed in Figure 4B or Figure 6SI, the response of the biosensor to increasing amounts of SARS-CoV-2 sequence decreases linearly (r^2=0.991) as the concentration of SARS-CoV-2 sequence increases in the studied range of concentration. The plot of biosensor response versus log [SARS-CoV-2_C] fits the linear equation ECL = -12.02 log [SARS-CoV-2_C] + 453.23 (R = 0.997). 3 Sb m^{-1} and 10 Sb m^{-1} criteria were used to calculate the limit of detection (LOD) and quantification (LOQ), where Sb is the standard deviation of the background signal ($Probe_{ORF}$-SH/AuNMs/AuSPE) and m is the slope of the calibration curve. The values estimated for the limit of detection (LOD) and quantification (LOQ) were found to be 720 aM and 40.2 fM, respectively.

The selectivity of the biosensor to detect specific sequences SARS-CoV-2 was also evaluated. In particular, we have studied the variation of the ECL signal in samples containing SARS-CoV-2 sequence (50.0 pM) in the absence and in the presence of other virus sequences as Influenza A (H7N9) and SARS-CoV-1, at the same concentration (50.0 pM). In both cases, the ECL signal obtained is quite similar to those obtained for SARS-CoV-2 sequence (see Figure 5SI). From these results, it can be concluded that the method can detect a target sequence of SARS-CoV-2 in presence of potential interfering sequences from other virus.

The reproducibility of the method was calculated using the response of three devices, prepared using the same protocol, fixing 50.0 pM as the analyte concentration sequence. The relative standard deviation (RSD) was found to be to be 0.82% and a repeatability of 99.36% obtained by measuring 5 times the biosensor response. Furthermore, the biosensor can detect the target SARS-CoV-2 at least over a period of one month.

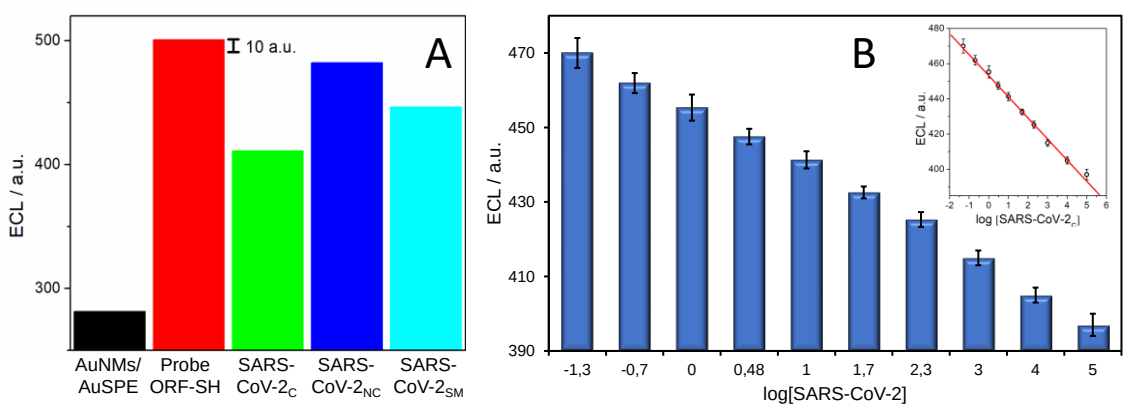

Figure 4. A) Bar diagrams of the ECL signal of AuNMs/AuSPE (black) and the biosensor response before (red) and after hybridization with 1.0 nM: complementary SARS-CoV-2_C (green), a non-complementary, SARS-CoV-2_{NC} (blue) and a mutated SARS-CoV-2_{SM} (cyan) sequences. B) Bar diagrams of the ECL biosensor response to increasing concentrations of the complementary sequence, SARS-CoV-2_C (from 50.0 fM to 100.0 nM). Inset: Calibration plot of the ECL signal *vs* log[SARS-CoV-2_C] concentration.

3.4. Mutation detection

The possibility of detecting SARS-CoV-2 variants is currently a great deal of interest. Hence, we have studied the possibility of detecting gene mutation using the developed biosensor. In particular, Single Nucleotide Polymorphism (SNPs) detection have been studied. Figure 4A shows the ECL biosensor responses recorded after hybridization with a 1.0 nM solution of a single-mismatched (SARS-CoV-2_{SM}) sequence (see Table 1). As can be seen, the biosensor response to the SNP containing sequence (SARS-CoV-2_{SM}) produces a decrease ECL signal of 50 ± 7 a.u, which is much lower than the observed for the complementary sequence (SARS-CoV-2_C) that produces a decrease of around 70 ± 5 a.u, confirming the high selectivity of the proposed biosensor.

3.5. SARS-CoV-2 determination in spiked human serum samples.

Finally, we evaluated the applicability of the biosensor by determining SARS-CoV-2 sequences in human serum samples. The ECL signal of the $[Ru(bpy)_3]^{2+}$/CDs ECL system obtained for a spiked human serum sample (final SARS-CoV-2 concentration of 50.0 pM) gave an average value of 430.2 ± 1.56 a.u. (see experimental section). From the calibration plot, the SARS-CoV-2 concentration in the spiked serum sample was found to be 54.1 pM with a recovery of 108% and a RSD of 5%. This result demonstrates that the developed biosensor can be applied for practical applications and has great potential as an alternative to the classical methods of SARS-CoV-2 detection in human samples.

Table 2. ECL and electrochemical DNA biosensors for SARS-CoV-2.

Target analyte	*Principle*	*Method*	*L.O.D*	*Reference*
26-nt-long ORF1ab fragment of SARS-CoV-2 RNA	Catalytic hairpin assembly	DPV	26 fM	[27]
25-nt-long ORF1ab fragment of SARS-CoV-2 RNA	MoS_2 and thionine-carbon nanodots	DPV	1.01 pM	[28]
COVID-19 N-gene	Electropolymerized polyaniline (PANI) nanowires and newly designed peptides	DPV	3.5 fM	[29]
ORF1ab from SARS-CoV-2	Supersandwich-type recognition strategy with calixarene	DPV	3 aM	[30]
SARS-CoV-2 RdRp	DNA tetrahedron with an entropy-driven reaction	ECL	2.67 fM	[8]
SARS-CoV-2 RdRp gene	DNA tetrahedrons of dual wavelength ratiometric by using entropy-driven and bipedal DNA walker amplification strategy	ECL	7.8 aM	[6]
SARS-CoV-2 RdRp gene	Au@Ti3C2@PEI-Ru(dcbpy)32+ nanocomposite	ECL	0.21 fM	[9]
ORF1ab fragment of SARS-CoV-2 RNA	AuNMs and CDs	ECL	514 aM	Present work

Table 2 shows ECL or electrochemical DNA biosensors described in the literature to detect SARS-CoV-2 sequences. As can be observed, the analytical parameters of the developed biosensor compare well with those previously reported in the literature. Moreover, the detection limit is comparable or even better and the developed biosensor is a simple, easy platform for SARS-CoV-2 detection. On the other hand, compared with other simple methodologies as colorimetric assay [31], the proposed biosensor present

lower detection limit proving a simple great practical alternative for detecting SARS-CoV-2 with low detection limit.

4. Conclusions

The use of gold nanomaterials (AuNMs) in combination with $[Ru(bpy)_3]^{2+}$/CDs system has been proved as a new strategy to develop new electrochemiluminescent nanostructured biosensor for the selective and sensitive assay of SARS-CoV-2 virus DNA sequences. AuNMs allow the immobilization of the thiolated DNA capture probe, which recognized DNA sequences related to the virus. The hybridization detection is achieved by using $[Ru(bpy)_3]^{2+}$/CDs that, in combination with AuNMs, enhance the sensitivity of the platform. The system is able to detect not only SARS-CoV-2 sequences with a detection limit of 514 aM but also SNPs in the virus sequence.

5. Acknowledgments

This work has been financially supported by the Spanish Ministry of Economy and Competitiveness (PID2020-116728RB-I00, CTQ2015-71955-REDT (ELECTROBIONET)) and Community of Madrid (TRANSNANOAVANSENS, S2018/NMT-4349). RdC gratefully thanks support from Fundación IMDEA, UAM and Banco Santander (fondo supera 2020, convocatoria CRUE-CSIC-SANTANDER, project with reference 10.01.03.02.41).

6. References

[1] WHO Director-General's opening remarks at the media briefing on COVID-19 - 11 March 2020, (2020). https://www.who.int/director-general/speeches/detail/who-director-general-s-opening-remarks-at-the-media-briefing-on-covid-19---11-march-2020 (accessed June 11, 2021).

[2] D.S. Chauhan, R. Prasad, R. Srivastava, M. Jaggi, S.C. Chauhan, M.M. Yallapu, Comprehensive Review on Current Interventions, Diagnostics, and Nanotechnology Perspectives against SARS-CoV-2, Bioconjugate Chem. 31 (2020) 2021–2045. https://doi.org/10.1021/ACS.BIOCONJCHEM.0C00323.

[3] A.R. Márquez-Ipiña, E. González-González, I.P. Rodríguez-Sánchez, I.M. Lara-Mayorga, L.A. Mejía-Manzano, M.G. Sánchez-Salazar, J.G. González-Valdez, R. Ortiz-López, A. Rojas-Martínez, G.T. Santiago, M.M. Alvarez, Serological Test to Determine Exposure to SARS-CoV-2: ELISA Based on the Receptor-Binding Domain of the Spike Protein (S-

RBDN318-V510) Expressed in Escherichia coli, Diagnostics 2021, Vol. 11, Page 271. 11 (2021) 271. https://doi.org/10.3390/DIAGNOSTICS11020271.

[4] A. Samacoits, P. Nimsamer, O. Mayuramart, N. Chantaravisoot, P. Sitthi-amorn, C. Nakhakes, L. Luangkamchorn, P. Tongcham, U. Zahm, S. Suphanpayak, N. Padungwattanachoke, N. Leelarthaphin, H. Huayhongthong, T. Pisitkun, S. Payungporn, P. Hannanta-anan, Machine Learning-Driven and Smartphone-Based Fluorescence Detection for CRISPR Diagnostic of SARS-CoV-2, ACS Omega. 6 (2021) 2727–2733. https://doi.org/10.1021/ACSOMEGA.0C04929.

[5] S. Suleman, S.K. Shukla, N. Malhotra, S.D. Bukkitgar, N.P. Shetti, R. Pilloton, J. Narang, Y. Nee Tan, T.M. Aminabhavi, Point of care detection of COVID-19: Advancement in biosensing and diagnostic methods, Chem. Eng. J. 414 (2021) 128759. https://doi.org/10.1016/J.CEJ.2021.128759.

[6] Z. Fan, B. Yao, Y. Ding, D. Xu, J. Zhao, K. Zhang, Rational engineering the DNA tetrahedrons of dual wavelength ratiometric electrochemiluminescence biosensor for high efficient detection of SARS-CoV-2 RdRp gene by using entropy-driven and bipedal DNA walker amplification strategy, Chem. Eng. J. 427 (2022) 131686. https://doi.org/10.1016/J.CEJ.2021.131686.

[7] S. Chen, C. Liu, Y. Liu, Q. Liu, M. Lu, S. Bi, Z. Jing, Q. Yu, W. Peng, Label-Free Near-Infrared Plasmonic Sensing Technique for DNA Detection at Ultralow Concentrations, Adv. Sci. 7 (2020). https://doi.org/10.1002/ADVS.202000763.

[8] Z. Fan, B. Yao, Y. Ding, J. Zhao, M. Xie, K. Zhang, Entropy-driven amplified electrochemiluminescence biosensor for RdRp gene of SARS-CoV-2 detection with self-assembled DNA tetrahedron scaffolds, Biosens. Bioelectron. 178 (2021) 113015. https://doi.org/10.1016/J.BIOS.2021.113015.

[9] B. Yao, J. Zhang, Z. Fan, Y. Ding, B. Zhou, R. Yang, J. Zhao, K. Zhang, Rational Engineering of the DNA Walker Amplification Strategy by Using a Au@Ti3C2@PEI-Ru(dcbpy)32+ Nanocomposite Biosensor for Detection of the SARS-CoV-2 RdRp Gene, ACS Appl. Mater. Interfaces. 13 (2021) 19816–19824. https://doi.org/10.1021/ACSAMI.1C04453.

[10] Y. Sun, P. Li, Y. Zhu, X. Zhu, Y. Zhang, M. Liu, Y. Liu, In situ growth of TiO2 nanowires on Ti3C2 MXenes nanosheets as highly sensitive luminol electrochemiluminescent nanoplatform for glucose detection in fruits, sweat and serum samples, Biosens. Bioelectron. 194 (2021) 113600. https://doi.org/10.1016/J.BIOS.2021.113600.

[11] X. Ma, W. Gao, F. Du, F. Yuan, J. Yu, Y. Guan, N. Sojic, G. Xu, Rational Design of Electrochemiluminescent Devices, Acc. Chem. Res. 54 (2021) 2936–2945. https://doi.org/10.1021/ACS.ACCOUNTS.1C00230.

[12] W. Miao, Electrogenerated Chemiluminescence and Its Biorelated Applications, Chem. Rev. 108 (2008) 2506–2553. https://doi.org/10.1021/CR068083A.

[13] Y.-M. Long, L. Bao, J.-Y. Zhao, Z.-L. Zhang, D.-W. Pang, Revealing Carbon Nanodots As Coreactants of the Anodic Electrochemiluminescence of Ru(bpy)32+, Anal. Chem. 86 (2014) 7224–7228. https://doi.org/10.1021/AC502405P.

[14] V. Strauss, J.T. Margraf, K. Dirian, Z. Syrgiannis, M. Prato, C. Wessendorf, A. Hirsch, T. Clark, D.M. Guldi, Carbon Nanodots: Supramolecular Electron Donor–Acceptor Hybrids

Featuring Perylenediimides, Angew. Chem., Int. Ed. 54 (2015) 8292–8297. https://doi.org/10.1002/ANIE.201502482.

[15] V. Strauss, J.T. Margraf, C. Dolle, B. Butz, T.J. Nacken, J. Walter, W. Bauer, W. Peukert, E. Spiecker, T. Clark, D.M. Guldi, Carbon Nanodots: Toward a Comprehensive Understanding of Their Photoluminescence, J. Am. Chem. Soc. 136 (2014) 17308–17316. https://doi.org/10.1021/JA510183C.

[16] W. Zhao, Y. Wang, K. Liu, R. Zhou, C. Shan, Multicolor biomass based carbon nanodots for bacterial imaging, Chin. Chem. Lett.. (2021). https://doi.org/10.1016/J.CCLET.2021.08.084.

[17] J. Shen, S. Shang, X. Chen, D. Wang, Y. Cai, Facile synthesis of fluorescence carbon dots from sweet potato for Fe3 + sensing and cell imaging, Mater. Sci. Eng., C. 76 (2017) 856–864. https://doi.org/10.1016/J.MSEC.2017.03.178.

[18] R. Abedi, J. Bakhsh Raoof, A. Bagheri Hashkavayi, M. Asghary, Highly sensitive and label-free electrochemical biosensor based on gold nanostructures for studying the interaction of prostate cancer gene sequence with epirubicin anti-cancer drug, Microchem. J. 170 (2021). https://doi.org/10.1016/J.MICROC.2021.106668.

[19] A.C.R. Moço, J.A.S. Neto, D.D. de Moraes, P.H. Guedes, J.G. Brussasco, J.M.R. Flauzino, L.F.G. Luz, M.M.C.N. Soares, J.M. Madurro, A.G. Brito-Madurro, Carbon ink-based electrodes modified with nanocomposite as a platform for electrochemical detection of HIV RNA, Microchem. J. 170 (2021) 106739. https://doi.org/10.1016/J.MICROC.2021.106739.

[20] Y. Niu, J. Liu, W. Chen, C. Yin, W. Weng, X. Li, X. Wang, G. Li, W. Sun, A direct electron transfer biosensor based on a horseradish peroxidase and gold nanotriangle modified electrode and electrocatalysis, Anal. Methods. 10 (2018) 5297–5304. https://doi.org/10.1039/C8AY01980K.

[21] I. Horcas, R. Fernández, J.M. Gómez-Rodríguez, J. Colchero, J. Gómez-Herrero, A.M. Baro, WSXM: A software for scanning probe microscopy and a tool for nanotechnology, Rev. Sci. Instrum. 78 (2007) 13705. https://doi.org/10.1063/1.2432410.

[22] B. Pelaz, V. Grazu, A. Ibarra, C. Magen, P. del Pino, J.M. de La Fuente, Tailoring the synthesis and heating ability of gold nanoprisms for bioapplications, Langmuir. 28 (2012) 8965–8970. https://doi.org/10.1021/la204712u.

[23] L. Gutiérrez-Gálvez, T. García-Mendiola, C. Gutiérrez-Sánchez, T. Guerrero-Esteban, C. García-Diego, I. Buendía, · M Laura García-Bermejo, · Félix Pariente, E. Lorenzo, Carbon nanodot–based electrogenerated chemiluminescence biosensor for miRNA-21 detection, Microchim. Acta. 2021 188:11. 188 (2021) 1–12. https://doi.org/10.1007/S00604-021-05038-Y.

[24] P. Miao, T. Zhang, J. Xu, Y. Tang, Electrochemical Detection of miRNA Combining T7 Exonuclease-Assisted Cascade Signal Amplification and DNA-Templated Copper Nanoparticles, Anal. Chem. 90 (2018) 11154–11160. https://doi.org/10.1021/ACS.ANALCHEM.8B03425.

[25] X. Jiang, Y. Chai, H. Wang, R. Yuan, Electrochemiluminescence of luminol enhanced by the synergetic catalysis of hemin and silver nanoparticles for sensitive protein

detection, Biosens. Bioelectron. 54 (2014) 20–26. https://doi.org/10.1016/J.BIOS.2013.10.006.

[26] X. Liu, W. Niu, H. Li, S. Han, L. Hu, G. Xu, Glucose biosensor based on gold nanoparticle-catalyzed luminol electrochemiluminescence on a three-dimensional sol–gel network, Electrochem. Commun. 10 (2008) 1250–1253. https://doi.org/10.1016/J.ELECOM.2008.06.009.

[27] Y. Peng, Y. Pan, Z. Sun, J. Li, Y. Yi, J. Yang, G. Li, An electrochemical biosensor for sensitive analysis of the SARS-CoV-2 RNA, Biosens. Bioelectron. 186 (2021) 113309. https://doi.org/10.1016/j.bios.2021.113309.

[28] E. Martínez-Periñán, T. García-Mendiola, E. Enebral-Romero, R. del Caño, M. Vera-Hidalgo, M. Vázquez Sulleiro, C. Navío, F. Pariente, E.M. Pérez, E. Lorenzo, A MoS2 platform and thionine-carbon nanodots for sensitive and selective detection of pathogens, Biosens. Bioelectron. 189 (2021) 113375. https://doi.org/10.1016/j.bios.2021.113375.

[29] Z. Song, Y. Ma, M. Chen, A. Ambrosi, C. Ding, X. Luo, Electrochemical Biosensor with Enhanced Antifouling Capability for COVID-19 Nucleic Acid Detection in Complex Biological Media, Anal. Chem. 93 (2021) 5963–5971. https://doi.org/10.1021/acs.analchem.1c00724.

[30] H. Zhao, F. Liu, W. Xie, T.C. Zhou, J. OuYang, L. Jin, H. Li, C.Y. Zhao, L. Zhang, J. Wei, Y.P. Zhang, C.P. Li, Ultrasensitive supersandwich-type electrochemical sensor for SARS-CoV-2 from the infected COVID-19 patients using a smartphone, Sens. Actuators, B. 327 (2021) 128899. https://doi.org/10.1016/j.snb.2020.128899.

[31] M. Wang, Y. Lin, J. Lu, Z. Sun, Y. Deng, L. Wang, Y. Yi, J. Li, J. Yang, G. Li, Visual naked-eye detection of SARS-CoV-2 RNA based on covalent organic framework capsules, Chem. Eng. J. 429 (2022) 132332. https://doi.org/10.1016/J.CEJ.2021.132332.